

LA-UR- 09-03680

Approved for public release;  
distribution is unlimited.

<i>Title:</i>	Calculations of Turbidite Deposits and Tsunamis from Submarine Landslides
<i>Author(s):</i>	Galen Gisler, Robert Weaver and Michael Gittings
<i>Intended for:</i>	Conference on Submarine Mass Movement and their Consequences, Austin TX November 2009



Los Alamos National Laboratory, an affirmative action/equal opportunity employer, is operated by the Los Alamos National Security, LLC for the National Nuclear Security Administration of the U.S. Department of Energy under contract DE-AC52-06NA25396. By acceptance of this article, the publisher recognizes that the U.S. Government retains a nonexclusive, royalty-free license to publish or reproduce the published form of this contribution, or to allow others to do so, for U.S. Government purposes. Los Alamos National Laboratory requests that the publisher identify this article as work performed under the auspices of the U.S. Department of Energy. Los Alamos National Laboratory strongly supports academic freedom and a researcher's right to publish; as an institution, however, the Laboratory does not endorse the viewpoint of a publication or guarantee its technical correctness.

# Calculations of Turbidite Deposits and Tsunamis from Submarine Landslides

Galen Gisler

Physics of Geological Processes, University of Oslo

Robert P Weaver

Los Alamos National Laboratory

Michael Gittings

Science Applications International

## Abstract

Great underwater landslides like Storegga off the Norwegian coast leave massive deposits on the seafloor and must produce enormous tsunamis. Such events have occurred on continental slopes worldwide, and continue to do so. Triggers for such slides include earthquakes, gas hydrate releases, and underwater volcanos. We have performed a numerical study of such landslides using the multi-material compressible hydrocode Sage in order to understand the relationship between the rheology of the slide material, the configuration of the resulting deposits on the seafloor, and the tsunami that is produced. Instabilities in the fluid-fluid mixing between slide material and seawater produce vortices and swirls with sizes that depend on the rheology of the slide material. These dynamical features of the flow may be preserved as ridges when the *sliding material* finally stops. Thus studying the configuration of the ridges in prehistoric slides may give us measures of the circumstances under which the slide was initiated. As part of this study, we have also done a convergence *test* showing that the slide velocity is sensitive to the resolution adopted in the simulation, but that extrapolation to infinite resolution is possible, and can yield good velocities. We will present two-dimensional simulations of schematic underwater slides for our study of rheology, and a three-dimensional simulation in bathymetric conditions that resemble the pre-Storegga Norwegian margin.

## 1. Introduction

Submarine landslides may of course be triggered by earthquakes, or they may have other causes, such as increased sediment load at the top of a continental shelf or a change in thermal conditions that moves deposited hydrates out of their regime of stability. We are interested in the relics deposited by the landslides on the seafloor, and wish to determine whether examination of such deposits could yield some understanding as to the rheology of the landslide (Wynn & Masson 2003). The characteristics of the tsunami resulting from an underwater landslide depend on the slide rheology. The stiffer the slide, the more energy is consumed in heating up the slide material, the substrate, and the water, and the less energy is therefore available to convert into tsunami energy. In considering the potential dangers from submarine landslides, it is therefore of interest to determine the rheology of the material that

would be involved in the landslide.

The energetic considerations can be derived from examining the physical configuration immediately before a landslide, and comparing to the configuration long afterwards, when the sea is again calm. The only difference is the location of the slide material: resting on the continental slope (for example) before the slide, and resting on the seafloor afterwards. Thus the free energy which drives the dynamics of the event (landslide plus tsunami) is the gravitational potential energy of the slide material at its initial height above the seafloor. As the slide begins, some of this potential energy is converted to kinetic energy as the material starts to move down the slope. Almost immediately, it begins to share this kinetic energy with the water, pushing the water ahead up and out of the way, and sucking the water behind downwards. Friction between the sliding material and the base heats up both, and entrainment of the water into eddies at the interface between slide and water leads to dissipation of the kinetic energy, further heating the slide material, and heating the water as well. The water sucked downwards behind the slide, and pushed upwards ahead of the slide represents a dipole wave source, which then radiates away with a directed pattern. Nearby shores, upstream of the continental slope, will experience a leading trough, while shores on the opposite side will experience a leading crest. If the wave amplitude is large, it will also interact with the atmosphere, thereby losing additional kinetic energy.

The system therefore consists of slide material, water, base, and atmosphere: four different materials with different mechanical properties. The best way to study such a system numerically is by using a multi-phase multi-material dynamical code.

## 2. The Sage code

We use an adaptive grid Eulerian code known as Sage (Gittings et al. 2006), developed for the US Department of Energy's program in Advanced Simulation and Computing by Los Alamos National Laboratory and Science Applications International. Sage is a compressible hydrocode with a high-resolution Godunov scheme and continuous adaptive mesh refinement. The equations solved are the continuity equation,

$$\frac{\partial \rho}{\partial t} + \nabla \cdot (\rho \mathbf{v}) = 0; \quad (1)$$

the equation for the conservation of momentum,

$$\frac{\partial \rho \mathbf{v}}{\partial t} + \nabla \cdot \rho \mathbf{v} \mathbf{v} + \nabla \cdot \boldsymbol{\sigma} = 0; \quad (2)$$

and for the conservation of energy,

$$\frac{\partial \rho \varepsilon}{\partial t} + \nabla \cdot (\rho \varepsilon \mathbf{v}) + \nabla \cdot (\boldsymbol{\sigma} \mathbf{v}) = 0. \quad (3)$$

The symbols in these equations have their usual meanings:  $\rho$  is density,  $\mathbf{v}$  is the fluid velocity,  $\boldsymbol{\sigma}$  the stress tensor (the trace of which is the thermodynamic pressure), and  $\varepsilon$  is the internal energy per unit mass. These are simply the Euler equations of compressible fluid flow, with the full stress tensor in equations (2) and (3) replacing the usual pressure variable in order to treat materials such as solids that can support asymmetric stresses. These must be supplemented with an appropriate prescription for gravity, dependent on geometry, and closed with a constitutive equation expressing the relation among the stress state, internal

energy, and density, for each material in the problem. The constitutive relation for materials that do not support transverse stresses is simply a thermodynamic equation of state, but for elastic solids and plastically flowing materials more equations must be added. A wide variety of equations of state and constitutive relations, both analytical and tabular, are available within the code.

Each cell in the computational volume can contain, in principle, all the materials defined in the problem. At the beginning of a computational cycle, Sage computes partial stresses, internal energies, and densities for all materials in a cell. With the assumption of local thermodynamic equilibrium within a cell, a unique cell temperature is defined, and momentum conservation serves to define a unique velocity associated with the cell.

### 3. Problem setup for submarine landslide calculations

The problem we consider here has effectively four materials: air for the atmosphere, water for the ocean, a weak basalt for the sliding material, and a strong basalt for the basement. We use tabular equations of state from the LANL Sesame library (Holian 1984; Lyon and Johnson 1992) for air and basalt, and for water we use an equation of state provided by Science Applications International as part of the Sage package. For the basalt we use a simple analytical elastic-perfectly plastic strength model, characterised by a yield strength, a shear modulus, and a fail pressure (the bulk modulus comes out of the Sesame tabular equation of state). The strong basalt used for the seafloor is given a yield strength of 1 Mbar, so that it behaves elastically throughout the calculation and does not move. The basalt used for the sliding material has a nominal yield strength of only 1 bar, and begins to shift under its own weight as soon as the calculation begins. The shear modulus for the sliding material is varied, over the six runs we report here, from 1 bar to 3 kbar (see Table 1). All of these runs are two-dimensional, effectively infinite in extent in the plane perpendicular to the calculation.

Table 1. Input and output characteristics of seven submarine landslide runs.

	<b>shear modulus of slide material (bar)</b>	<b>near-field tsunami amplitude (m)</b>	<b>free energy into water kinetic energy (%)</b>	<b>free energy into heating of water and slide (%)</b>
<b>SGrYa</b>	1	100	5.6	57
<b>SGrZa</b>	10	100	5.0	58
<b>SGr0a</b>	100	91	3.9	59
<b>SGr1a</b>	300	80	3.1	61
<b>SGr2a</b>	1000	64	1.9	63
<b>SGr3a</b>	3000	45	1.4	67

All of the runs have identical starting configurations, as illustrated in Fig. 1. The vertical extent of the computational volume is 6 km, of which 2 km is above the ocean surface. The horizontal extent is 100 km, of which half is shown in Fig. 1. The basement

consists of a continental shelf of 2-degree slope, starting 100 m below the ocean surface at the left boundary, and ending at a depth of 600 m and a distance of 14.3 km from the boundary. The continental slope inclines from there with a slope of 9 degrees, ending on the abyssal plain at 4.5 km depth and 39.9 km from the boundary. The abyssal plain then continues down towards the right with a slope of 0.5 degrees, reaching a depth of 5 km at the right boundary. The slide material is a quadrilateral region cut out from the shelf and slope, starting at a depth of 300 m and a distance 5.73 km from the left boundary, with the slide plane having an average slope of 7 degrees. The toe of the slide material is at 3.96 km depth, 35.5 km from the boundary, and the cut point is at 1.3 km depth, 12 km from the boundary.

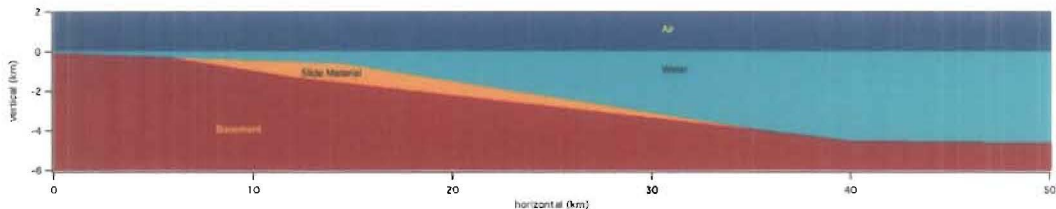


Fig. 1. Initial configuration for the runs of Table 1. The full vertical extent of the computational volume is shown, but only half the horizontal extent. There are four materials in the problem, as labeled here. Both the basement and the slide material are basalt, but while the basement basalt is made very strong, the slide material basalt is made weak enough that it begins to flow under its own weight as soon as the calculation begins. An initial hydrostatic equilibrium is calculated at the right end of the box and used to initialize pressures throughout the calculation.

The acceleration due to gravity is the standard earth value of  $980 \text{ cm/s}^2$ , and pressures throughout the problem are initialized by calculation of isothermal hydrostatic equilibrium on the right boundary, which is therefore a column of 2 km air, 5 km water, and 1 km basalt, constrained by the requirement that the pressure at the water surface is 1 bar. This procedure produces initialization pressures that are too low within the basalt basement on the left, but since the basalt is strong and elastic, the adjustment is made rapidly (within  $\sim 25$  sec) once the dynamic calculations are underway, and the calculation results are not substantially affected.

#### 4. The calculations

A sequence of density plots from run SGrYa, the run with the most mobile (nearly inviscid) slide material, is shown in Figure 2. A horizontal line is drawn at the position of the original sea surface, so that it is possible to see the initial draw-down of the water as the landslide begins. The elevation of the water ahead of the slide bullnose is not visually apparent on the figure because it is of much lower amplitude. The minimum cell size in these calculations is 15 m, invisible on the figure.

The ripples on the interface between the slide material and the water are due to a two-stream, or Kelvin-Helmholtz instability. By the bottom frame in Fig. 2, at 300 seconds, the ripples at the head of the slide have evolved into turbidity currents, of a depth larger than or comparable to the original slide depth. Substantial mixing between water and slide material is taking place, and it would be anticipated that a slide like this would leave a relic on the seafloor having numerous ridges as remnants of the turbidity currents.

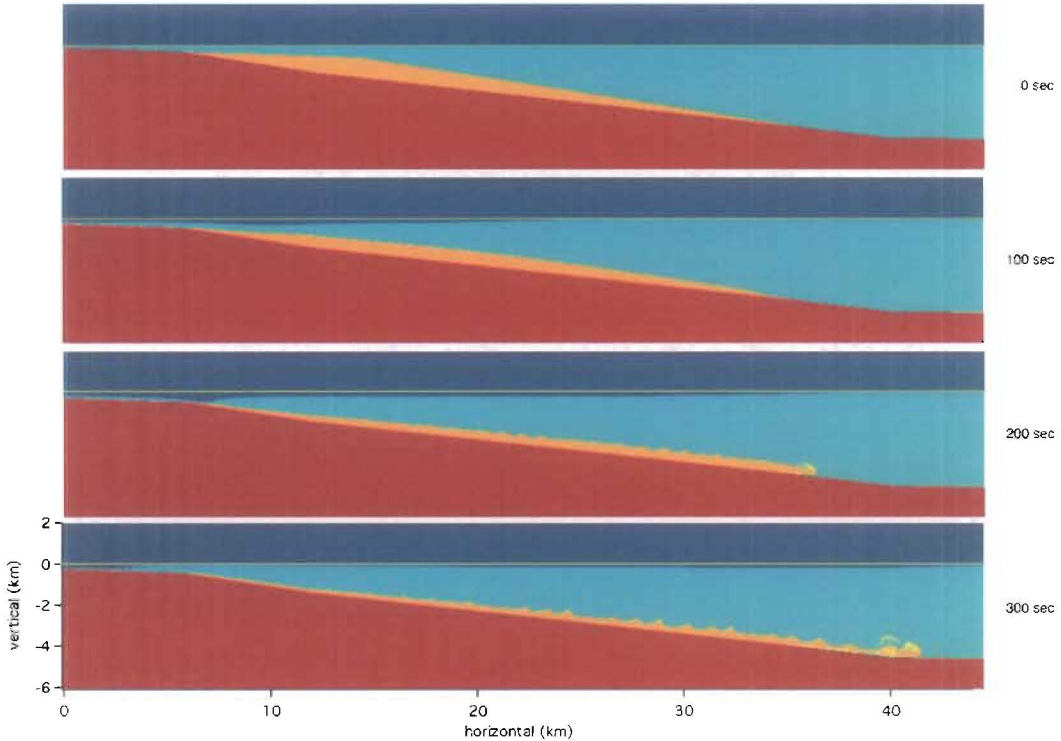


Fig. 2. Snapshots from the first 300 seconds of run SGrYa of Table 1. The weak material of the slide region begins to move under its own weight at the beginning of the calculation. After a minute and a half, there is already a substantial drawdown of the water surface above the head of the slide. Ripples start to form on the interface between slide and water by about 3 minutes, and by the time the head of the slide has reached the bottom of the slope, these ripples have become strong turbidity currents. Meanwhile water rushes in to fill the drawdown at the slide head and moves towards shore on the left, and the leading crest of the tsunami has moved off to the right.

In Figure 3 we show the energy evolution in this run. The slide's motion, beginning at the start of the calculation, is reflected in the rise of its kinetic energy curve over the first few minutes as the slide material's potential energy is converted first into kinetic energy and then into heat. At about 3 minutes, the slide kinetic energy peaks and is roughly equalled by the slide heat energy, which continues to rise. The water, partly pushed out of the way by the slide, and partly entrained by it, is simultaneously heated and accelerated, until after about 6 minutes when heating begins to dominate. After this point the water loses kinetic energy very slowly as the wave propagates away from the source. After about 550 seconds, the leading edge of the disturbance starts to leave the computational volume, and the kinetic energy of the water retained in the volume drops accordingly. The slide decelerates strongly through friction with the bottoms and resistance from the water. The calculation was terminated at 800 seconds, by which time heat inputs have saturated. The fraction of the slide material's initial potential energy that is transferred to the water's kinetic energy is less than 6%, as shown in Table 1, while over half the energy has gone into heating the water and the slide material. The missing energy goes mainly into heating the basement, and a small fraction into motion of the air.

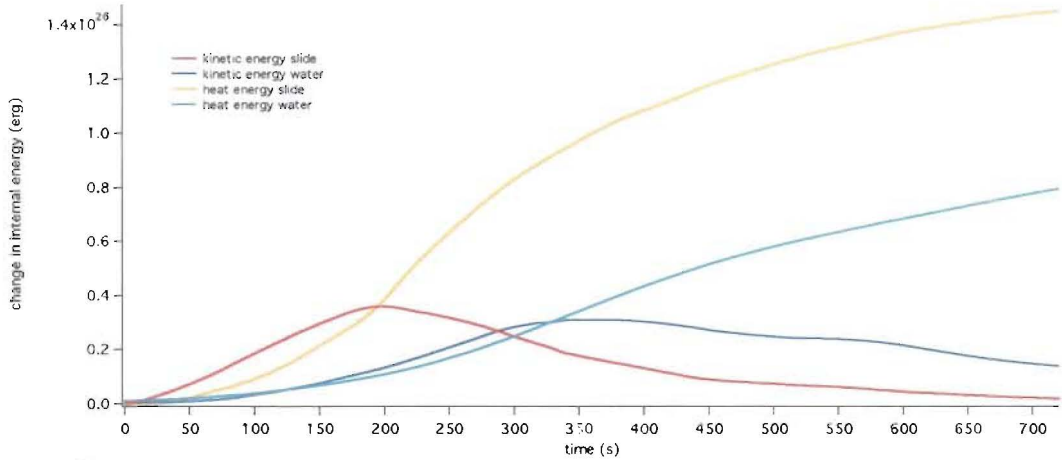


Fig. 3. Energy evolution for run SGrYa of Table 1. Plotted are kinetic energy of the slide material and water, and heat (internal) energy of the slide material and water, as a function of physical time in the calculation. The slide material acquires a great deal more heat energy than kinetic energy, even as it decelerates to a stop. The water acquires heat energy as rapidly as it does kinetic energy, and continues being heated after its kinetic energy saturates. The decline in water kinetic energy after 350 s is very slow and then becomes more rapid as the oscillatory wave motion in the water gradually moves out of the box.

In Figure 4 we show simultaneous snapshots of the other five runs of Table 1, at a uniform time of 400 seconds for all runs. The dark vertical line is at the position where the continental slope meets the abyssal plane. The slide material in run SGr2a has just reached this point, while the stiffer slide material in SGr3a lags behind, and the less stiff runs above have all passed it by. The runnier slides differ from the stiffer slides also in having a bumpier interface with the water. This difference persists to the end of the calculations in these runs, and presumably is preserved to some extent long after the slide comes to rest on the seafloor. Finally, the runnier slides produce higher amplitude tsunamis, as seen in the numbers in Table 1, but also in the visually noticeable difference in the shoreward propagating wave on the left-hand side, above the continental shelf.

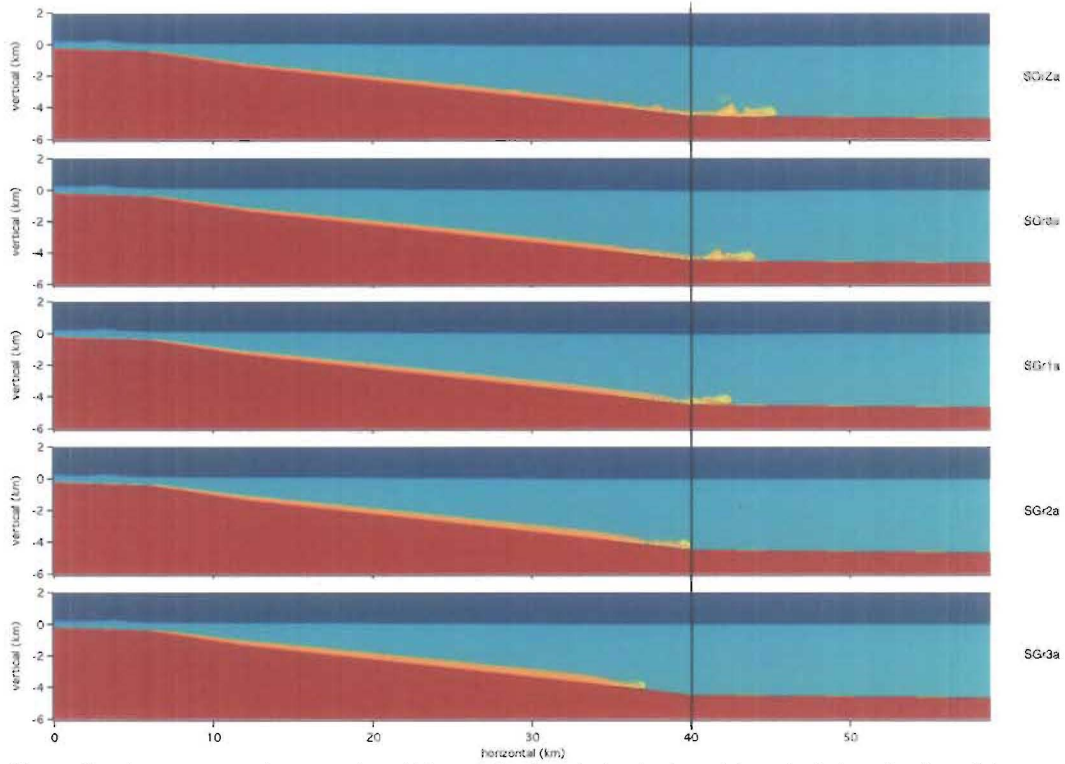


Fig. 4. Simultaneous snapshots at a time 400 seconds after the beginning of the calculations for five of the runs of Table 1. Run SG0a is omitted, since its configuration at 300 seconds is shown in Figure 3. The stiffest calculations are at the bottom, the runniest at the top. The dark vertical line, to guide the eye, is placed where the continental slope meets the abyssal plain. The runniest slides produce more turbidity currents and will leave bumpier relics on the seafloor.

The tsunami amplitudes quoted in Table 1 are derived from analysis of tracer particle trajectories. At the beginning of the calculation, 200 massless Lagrangian tracer particles are distributed on the surface of the water and 50 m below, between 10 km and 40 km from the left-hand edge of the computational volume. A trajectory plot of a sample of these tracers, from run SG0a, is shown in Figure 5. Each trajectory in this plot is colored by time, red at the beginning of the calculation, blue at the end. A typical tracer in this range (between 30 and 40 km out, close to the end of the continental slope) sits nearly stationary, drifting up and down with acoustic waves, until the tsunami passes. The particle then moves upward by about 50 m and outward by several hundred metres, then downward by about 150 m and backwards by several km as the refilling wave passes. Subsequent waves produce nearly in-place vertical motion. The arrival time of the wave at each tracer enables measurement of the outward-going tsunami velocity. We measure this between the midpoint and the bottom of the slope, at about 150 km/s. Above the abyssal plain, the tsunami speed should reach 200 m/s, from the shallow-water formula for the wave speed ( $= \sqrt{gD}$ , where  $g$  is the acceleration due to gravity and  $D$  the water depth).

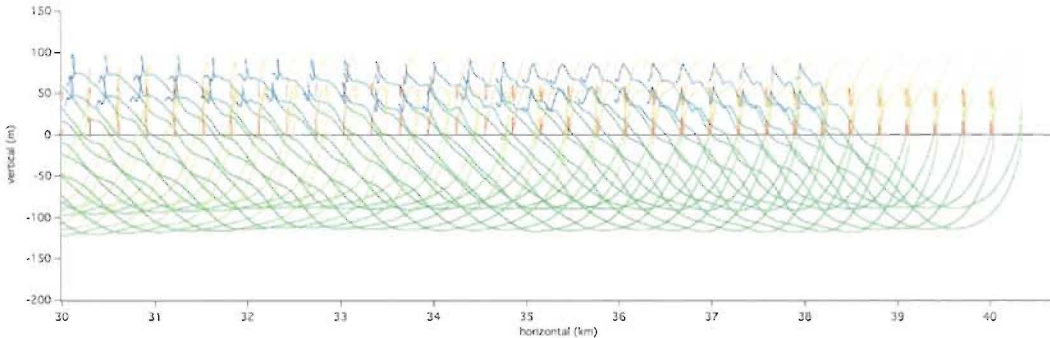


Fig. 5. Tracer particle trajectory plot for run SGr0a. Only trajectories between 30 and 40 km from the left-hand boundary are shown. Each particle's trajectory is colored to indicate physical time: red at the start of the calculation to blue at the calculation termination (800 s). For robustness, at each horizontal position we place two particles, one initially at the water surface, the other initially 50 m below. Particles start out nearly stationary, oscillating slightly with acoustic waves, until the tsunami reaches them. Then, typically, they make a slight motion outward and upward ( $\sim 50\text{m} \times 300\text{m}$ ) followed by a resurge motion downward and backward ( $150\text{m} \times 3000\text{m}$ ), and subsequently oscillate in place with the passage of subsequent waves.

Finally, numerical calculations being yet an imperfect art, we must examine the question of numerical resolution and how its practical limitation affects the conclusions we might draw from these calculations. In Figure 6 we show images from an earlier series of runs, in somewhat different, but similar geometry [note to reviewers: we intend to replace this figure with one more representative of the calculations we have performed for this paper before the final version is due. The highest-resolution run is still in progress at this moment]. These runs clearly show that the runout distance and the inferred degree of turbidity depend critically on resolution. Fortunately, it is possible to calculate a correct physical speed (and hence ultimate runout distance) at infinite resolution by taking the velocities as a function of smallest cell size and extrapolating down to zero cell size. Slide speed is found to increase as the spatial resolution is improved, suggesting that low speeds reported by previous numerical studies at lower resolution may be seriously in error. Please note that the resolution used for the runs of Table 1 is the same as that for the next-to-the-best run in Figure 6.

The roughness of the seafloor relic becomes harder to deal with in the extrapolation, however, since it is likely that the irregularities will go all the way down to dissipation scales or to the scale of the granularity of the slide medium, whichever is larger.

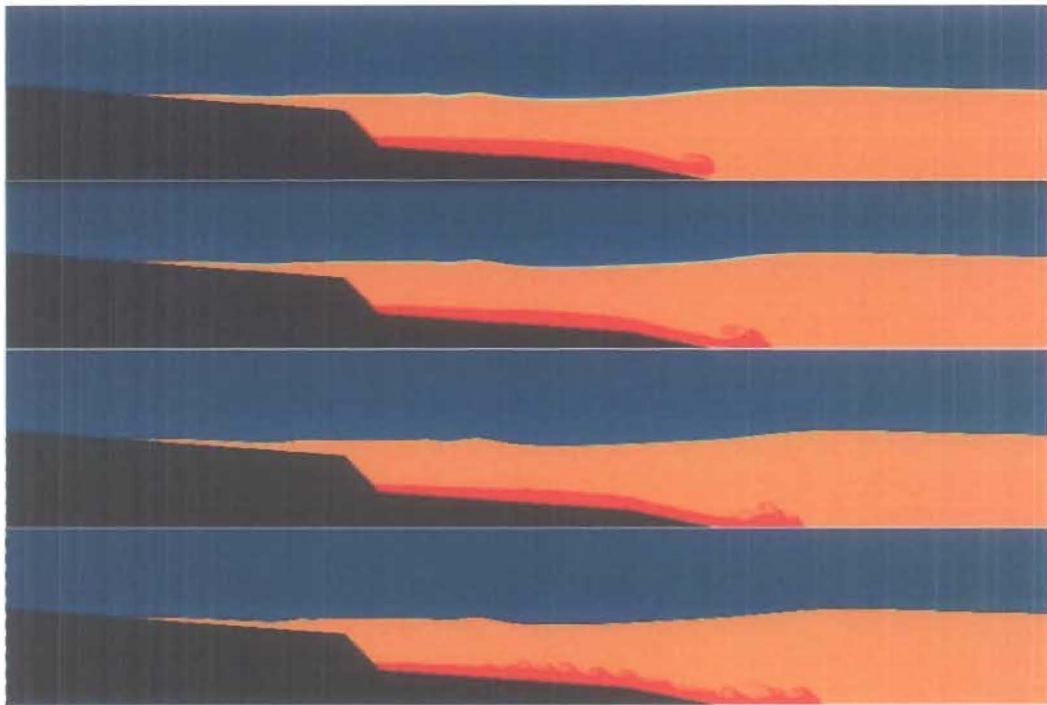


Fig. 6. Density raster plots for four two-dimensional runs of a submarine landslide with successively increasing spatial resolution at the same physical time after the slide start. The speed of the fluidized rock slide increases substantially as resolution improves, and the turbidity currents become more distinct and developed. The dimensions of the box are 10 km vertical by 60 km horizontal. From the top, the finest spatial resolution in the adaptively refined grid is 64 m, 32 m, 16 m, and 8 m. The average velocities of the toe of the slide are  $32 \text{ m s}^{-1}$ ,  $51 \text{ m s}^{-1}$ ,  $63 \text{ m s}^{-1}$ , and  $68 \text{ m s}^{-1}$ . Extrapolating to infinitely fine spatial resolution would give an average slide velocity of  $73 \text{ m s}^{-1}$ .

## 5. Discussion

The amplitude of a tsunami produced by an underwater landslide is dependent on many factors, one of which is the mobility of the sliding material. Runnier slides produce larger, more dangerous tsunamis, while stiffer slides produce more modest ones. Runnier slides also produce longer runouts, but at the same time leave more deposits from the turbidity currents that result in the interchange and mutual entrainment between slide material and water.

If slide mobility were the only variable, we would expect long-runout slide relics to be smoother than short ones. There are, however, other variables, including mode of failure (retrogressive or progressive), slide volume, initial topography, manner of fluidization, and so on. Viscosity may also vary within the slide itself, of course. A slide could have a nearly friction-free bottom layer and a relatively stiff upper layer and thereby produce a runout that is both long and very smooth. We have not attempted models of this sort yet.

Also, the degree to which slides of solid material, being in fact granular, act as a fluid is not directly addressed here. We suspect that the granularity might make the problem of smooth, long-runout landslide relics even more difficult.

## 6. Acknowledgments

We have benefited from fruitful discussions with tsunami experts all over the world, but especially with Charles Mader, who got us interested in this problem. Galen Gisler acknowledges the support of the Norwegian Research Council for the establishment and funding of PGP, a Norwegian Centre of Excellence in Research. The computing reported here has been done partly through resources provided by NOTUR, the Norwegian distributed supercomputing network, partly by ARSC, the Arctic Region Supercomputing Center in Fairbanks, Alaska, and partly at Los Alamos National Laboratory.

## References

Gisler, G.R., 2008. Tsunami simulations, *Annual Review of Fluid Mechanics*, **40**, 71-90.

Gittings M.L., Weaver R.P., Clover M., Betlach T., Byrne N., et al., 2006. The RAGE radiation-hydrodynamic code, *Los Alamos National Laboratory Report LA-UR-06-0027*, Los Alamos, New Mexico.

Holian, K.S., 1984. T-4 Handbook of material properties data bases: Vol 1c, equations of state, *Los Alamos National Laboratory Report LA-10610-MS*, Los Alamos, New Mexico.

Lyon, S.P., Johnson, J.D. 1992, Sesame: the Los Alamos National Laboratory equation of state database, *Los Alamos National Laboratory Report LA-UR-92-3407*, Los Alamos, New Mexico.

R. B. Wynn & D. G. Masson, “Canary Island landslides and tsunami generation: can we use turbidite deposits to interpret landslide processes?” pp325-332 in: *Submarine Mass Movements and their Consequences* (eds. J. Locat and J. Mienert). Kluwer Academic Publishers, Dordrecht, Boston, London, 2003.